Research Article

Journal of RAMAN SPECTROSCOPY

Received: 29 July 2011 Revised: 19 September 2011 Accepted: 28 September 2011 Published online in Wiley Online Library

(wileyonlinelibrary.com) DOI 10.1002/jrs.3094

# Raman investigation of silicon nanocrystals: quantum confinement and laser-induced thermal effects

Y. Duan,[a] J. F. Kong[b] and W. Z. Shen[a]*

**We present a detailed experimental and theoretical Raman investigation of quantum confinement and laser-induced local thermal effects on hydrogenated nanocrystalline silicon with different nanocrystal sizes (3.6–6.2 nm). The local temperature was monitored by measuring the Stokes/anti-Stokes peak ratio with the laser power density range from ~120 to 960 kW/cm$^2$. In combination with the three-dimensional phonon confinement model and the anharmonic effect, which incorporates the three-phonon and four-phonon decay processes, we revealed an asymmetrical decay process with wavenumbers ~170 and 350 cm$^{-1}$, an increasing anharmonic effect with nanocrystal sizes, and a shortening lifetime with enhanced temperature and decreasing nanocrystal dimension. Furthermore, we demonstrated experimentally that for Si nanocrystals smaller than 6 nm, the quantum confinement effect is dominant for the peak shift and line broadening. Copyright © 2011 John Wiley & Sons, Ltd.**

**Keywords:** silicon nanocrystals; thermal effect; quantum size effect; Raman spectra

**PACS numbers:** 78.30.Am, 65.80.–g, 63.20.–e, and 78.67.Bf.

## Introduction

Raman spectroscopy, as a fast, convenient, nondestructive, and highly sensitive probe of local atomic arrangements and vibrations, has been widely used to characterize the properties of nanomaterials including nanocrystals,[1–3] nanowires,[4] and microcrystalline structures.[5] The localization and lattice vibration properties of various low-dimensional semiconductor nanomaterials have been successfully yielded by the aid of detailed analyses of significant size-dependent red-shift and asymmetric broadening when the nanocrystal size is reduced to nanometer scale.[1,6–8] Many theoretical models have been established, such as the microscopic force model,[9] bond polarizable model,[10,11] and three-dimensional phonon confinement model,[12] to obtain a better interpretation of the experimental data. However, the local temperature of the nanostructured samples on the illuminated spot will increase even if the laser power is very low,[13] which can therefore affect significantly the vibrational properties.[6] Recently, Faraci *et al.*[3] have analyzed experimentally the quantum confinement and thermal effects of a 10-nm semiconductor nanocrystal as the laser power increases, and predicted theoretically the quantum confinement effect mainly for sizes smaller than ~6 nm.

It should be noted that there is no detailed study on the relationship between the Raman spectra related to the nanocrystal size and the thermal effect because of the laser irradiation. In fact, nanostructures are embedded in an environment medium, which can have poor thermal conductivity.[14] This establishes the base for the experimental determination of the local temperature through monitoring the Raman band shift[15] and the Stokes/anti-Stokes intensity ratio ($I_S/I_A$)[16] under different laser power densities. Therefore, the relationship between lattice vibration and thermal effect can be achieved straightforwardly. Moreover, a comprehensive investigation of the three-phonon and four-phonon decay processes[17] under laser irradiation is very important for the understanding of the phonon dynamic behavior in semiconductor nanostructures.

On the other hand, silicon nanostructures have attracted much attention in recent years because of their importance in the fundamental understanding of physics and potential applications in silicon optoelectronics.[18–20] In this paper, we present a detailed micro-Raman investigation of different silicon nanocrystal dimensions (3.6, 4.2, 5.0, and 6.2 nm) prepared by plasma enhanced chemical vapor deposition (PECVD) under the laser power density range from ~120 to 960 kW/cm$^2$. The average silicon nanocrystal dimensions were determined by the three-dimensional phonon confinement of Raman spectrum analysis. In combination with the effects of phonon confinement and anharmonic phonon processes, we clearly illustrate the temperature effect on the Raman peak shifts and linewidths. We demonstrate experimentally that for Si nanocrystals smaller than 6 nm, the quantum confinement effect is dominant for the Raman peak shift and line

* *Correspondence to: W. Z. Shen, Laboratory of Condensed Matter Spectroscopy and Opto-Electronic Physics, Key Laboratory of Artificial Structures and Quantum Control (Minister of Education), Department of Physics, Shanghai Jiao Tong University, 800 Dong Chuan Road, Shanghai 200240, China. E-mail: wzshen@sjtu.edu.cn*

a *Laboratory of Condensed Matter Spectroscopy and Opto-Electronic Physics, Key Laboratory of Artificial Structures and Quantum Control (Minister of Education), Department of Physics, Shanghai Jiao Tong University, 800 Dong Chuan Road, Shanghai 200240, China*

b *Department of Physics, Shanghai Institute of Technology, 100 Hai Quan Road, Shanghai 201418, China*

broadening. We further show that phonon dynamic behavior correlates with the phonon vibrational properties in nanoparticles.

## Experimental Details

The hydrogenated nanocrystalline Si (nc-Si:H) thin films employed for the current study were deposited on undoped crystalline Si (111) substrates at a temperature of 250 °C in a capacitive coupled PECVD system. During the growth, the total pressure of reactive gases was maintained at 0.7 Torr and the hydrogen dilution ratio $[H_2/(SiH_4+H_2)]$ at 99%, while the radio frequency (13.56 MHz) power changes from 30 to 90 W to achieve different nanocrystalline sizes. The nc-Si:H thin film is a mixed-phase material consisting of Si quantum dots embedded in amorphous Si tissue and has a layer thickness of around a few micrometers. The room-temperature electron mobility and dark conductivity of the nc-Si:H films reach in the order of $10^2$ cm$^2$/Vs and 10 Scm$^{-1}$, respectively.[21] The room-temperature Raman spectra were obtained by using a Jobin Yvon LabRam HR 800UV micro-Raman spectrometer with the 514.5 nm line of an $Ar^+$ laser. The employment of a 50× optical microscope objective with a numerical aperture of 0.75 will yield a laser spot size of ~2 μm. The scattered light was detected in a backscattering geometry of $z(x,-)\bar{z}$ configuration using an Andor DU420 classic charge-coupled device detector. The optical output power can be read from the meter of the laser system, and there is 25% power loss when it spreads in the light path. In this paper, the Raman spectra were recorded with the laser power in the range of 3.75 to 30.00 mW, corresponding to the laser power density between ~120 and 960 kW/cm$^2$.

## Results and Discussion

Figure 1 shows the typical Stokes and anti-Stokes Raman spectra taken from a nc-Si:H thin film with an average Si quantum dot size $d$ of 3.6 nm under five different laser power densities. It can be noted that the Raman spectra of nc-Si:H downshifts and asymmetrically broadens with increasing laser excitation power. In contrast to bulk Si,[22] the Raman spectra of nc-Si:H thin films are sensitive to the laser power density, which can be understood because of the poor thermal conductivity of nc-Si:H compared with the bulk Si. Because Si nanocrystals were embedded in an environment medium (amorphous Si matrix) as mentioned previously, the poor heat transfer between nanoparticles and weak thermal contact with the substrate result in low lattice thermal conductivity. Further evidence of the laser-induced thermal effect in the local area comes from the fact that the observed ratio of Stokes to anti-Stokes intensity $I_S/I_A$ decreases obviously with the increase of laser power density. As we know, $I_S/I_A \propto \exp(\hbar\omega/k_BT)$, with $\omega$ the local wavenumber and $T$ the local temperature, the significant decrease of $I_S/I_A$, together with the red-shift of the Stokes Raman peak, demonstrates the temperature rise of the local area with increasing laser power density. In addition, compared with the symmetric Lorentzian profile of the Raman lineshape in the bulk Si, the degree of asymmetry in the phonon peak of nc-Si:H increases with the decrease of dimension. The decreasing dimension causes lattice defect and structural disorder, which result in the breakdown of the translational symmetry at wave vector $q=0$, and the contribution of Brillouin zone edge phonons to participate in an inelastic Raman scattering process, i.e. greatly drives the lineshape asymmetry.

The average Si dot size $d$ can be yielded by calculating the Stokes and anti-Stokes Raman spectra. As an example in Fig. 2, we take the nc-Si:H sample for Fig. 1 with the laser power density of 120 kW/cm$^2$. The Raman scattering spectra can be interpreted by the combination of three Gaussian phonon bands [i.e. longitudinal acoustic (LA) band centered at 300 cm$^{-1}$, longitudinal optical (LO) band at 380 cm$^{-1}$, and transverse optical ($TO_1$) band at 480 cm$^{-1}$] from the amorphous Si contribution, and one asymmetric transverse optical ($TO_2$) band related to the Si nanocrystals.[23] To identify the asymmetry $TO_2$ peak of the Si nanocrystals, we employ the three-dimensional phonon confinement model[12] to detect the detailed temperature and size dependences of the phonon wavenumber and line broadening. According to the three-dimensional phonon confinement model, which

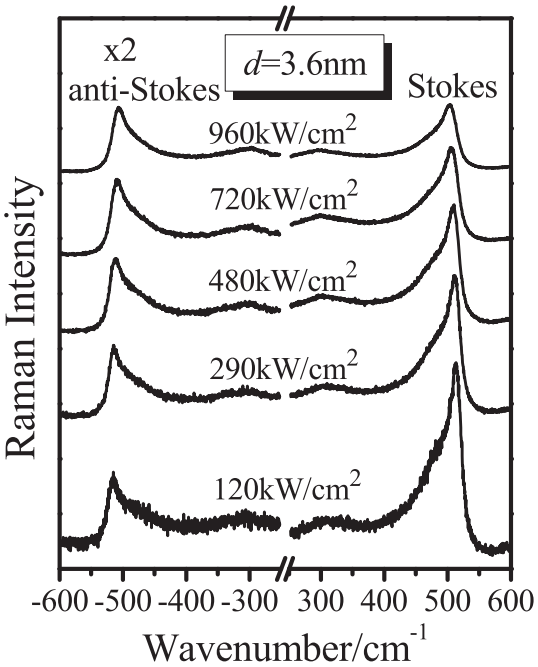


**Figure 1.** Stokes and anti-Stokes Raman spectra taken from a nc-Si:H thin film with an average Si quantum dot size $d$ of 3.6 nm under five different laser power densities.

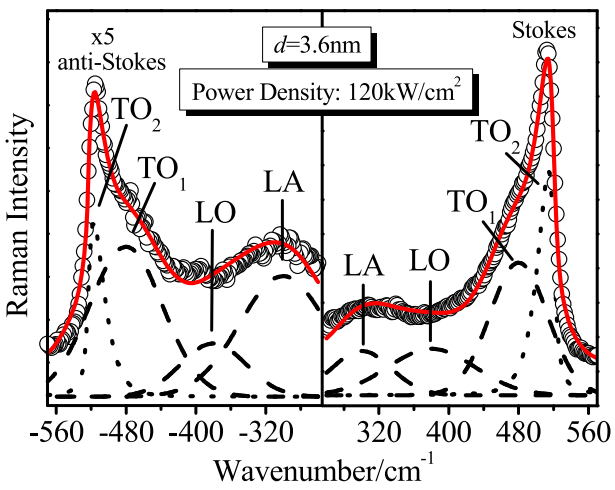


**Figure 2.** Experimental (open circles) and fitted (solid curves) Raman spectra for the nc-Si:H sample with grain size $d$ of 3.6 nm under the laser power density of 120 kW/cm$^2$. The dashed curves peaked at ~300, 380, and 480 cm$^{-1}$ correspond to LA, LO, and $TO_1$ modes of the amorphous Si, respectively. The dotted curve peaked at ~520 cm$^{-1}$ is related to the $TO_2$ mode of Si nanocrystals.

takes into account both the phonon confinement and the effect of strain, the $TO_2$ band Raman spectrum can be described as

$$I_{TO_2}(\omega) = I_{0_{Raman}} \int_0^{2\pi/a_0} \frac{|C(q)|^2 4\pi q^2 \cdot dq}{[\omega - \omega(q)]^2 + (\Gamma/2)^2} \quad (1)$$

with $I_{0_{Raman}}$ the prefactor, $|C(q)|^2=\exp(-q^2d^2/8)$ for spherical shape grain, $q$ the wave vector of phonon, $d$ the correlation length related to the average size of the Si nanocrystals, $\Gamma$ the Raman intrinsic linewidth of crystalline silicon, and $a_0 = 0.543$ nm the lattice constant of the bulk Si. The form of the phonon dispersion relation $\omega(q)$ is given by[24]

$$\omega(q) = \omega_p - 120(q/q_0)^2 \quad (2)$$

where $\omega_p$ is the wavenumber of the first order Raman band in the absence of disorder effects and $q_0 = 2\pi/a_0$.

We show in Fig. 2 the dotted curves for the calculated $TO_2$ peak of the Si nanocrystals and the dashed curves for the three Gaussian phonon bands from the amorphous Si contribution. Good agreement has been achieved in Fig. 2 between the calculated (solid curves) and experimental Raman spectra (circles). From the fitting, we can obtain the corresponding Si nanocrystal sizes and the strain of our nc-Si:H samples. As shown in Fig. 3 for the four nc-Si:H samples, there is some small variation for the yielded Si nanocrystal sizes under different laser power densities. In the present study, we have taken the mean values of 3.6, 4.2, 5.0, and 6.2 nm as the average Si dot sizes for the four samples within an accuracy of ±0.1 nm, which are in agreement with our observation from X-ray diffraction measurements and high-resolution transmission electron microscopy. In addition, the inhomogenetity of nanocrystal sizes are revealed by the three-dimensional phonon confinement model of the micro-Raman mapping spectra.[23] The strain is simply deduced from $-(\omega_p-\omega_0)/3\xi\omega_0$, with $\omega_0$ the wavenumber of the first-order Raman band in the absence of both disorder and stress effects (520.5 $cm^{-1}$) and $\xi$ the Grüneisen constant (~1.0).[23] The calculated intrinsic compressive strain with the laser power of 120 kW/$cm^2$ are listed in Table 1. Moreover, the local temperature was evaluated from the ratio of Stokes to anti-Stokes Raman intensity of the $TO_2$ mode under the laser power density in the range of ~120 to 960 kW/$cm^2$, with an estimated error of ±2 K. In the following,

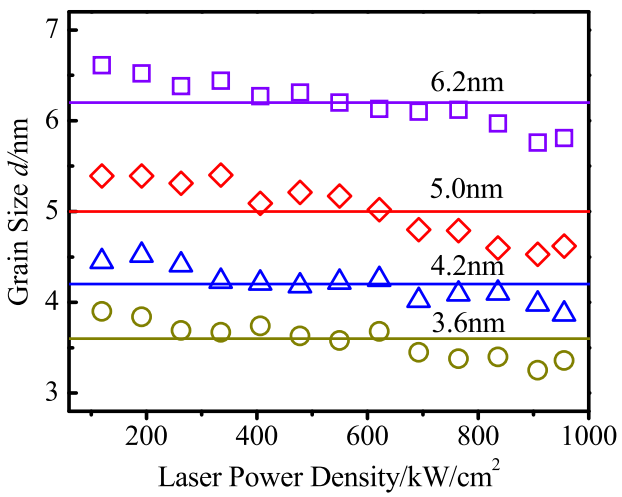


**Figure 3.** Yielded grain sizes from Raman spectra under different laser power densities.

**Table 1.** Parameters for fitting the Raman peak shift (Eqn (3)) and linewidths (Eqn (4)) of the $TO_2$ mode in Si nanocrystals, together with the yielded intrinsic compressive strain under the laser power of 120 kW/$cm^2$

| Grain size $d$ (nm) | $\omega_0$ ($cm^{-1}$) | $A$ ($cm^{-1}$) | $B$ ($cm^{-1}$) | $\Gamma_0$ ($cm^{-1}$) | $C$ ($cm^{-1}$) | $D$ ($cm^{-1}$) | Strain (×$10^{-3}$ Pa) |
|---|---|---|---|---|---|---|---|
| 3.6 | 521.30 | −1.73 | −0.22 | 6.86 | 0.34 | 0.045 | 2.07 |
| 4.2 | 524.91 | −1.75 | −0.23 | 5.83 | 0.36 | 0.047 | 2.32 |
| 5.0 | 526.75 | −1.80 | −0.24 | 4.86 | 0.39 | 0.051 | 2.84 |
| 6.2 | 528.08 | −1.82 | −0.25 | 3.31 | 0.42 | 0.054 | 3.16 |

we will concentrate on the temperature dependence of the Raman peak shift and line broadening of different Si dot sizes in terms of the model developed by Klemens,[25] Hart *et al.*,[16] and extended by Balkanski *et al.* [26] for anharmonic decay of optical phonons.

Figure 4 presents the Raman peak shift (scatters) of the $TO_2$ band as a function of the yielded local temperature for the four different average nanocrystal sizes. The phonon peaks $\omega(T)$ shift towards lower wavenumber in the same way with the increase in temperature, which can be expressed by taking into account cubic and quartic terms in the anharmonic Hamiltonian as[27]

$$\omega(T) = \omega_0 + \Delta\omega_{d1}(T) + \Delta\omega_{d2}(T)$$
$$\Delta\omega_{d1}(T) = A\left[1 + \frac{1}{\exp(\hbar\omega_1/k_BT) - 1} + \frac{1}{\exp(\hbar\omega_2/k_BT) - 1}\right]$$
$$\Delta\omega_{d2}(T) = B\left[1 + \frac{3}{\exp(\hbar\omega_0/3k_BT) - 1} + \frac{3}{[\exp(\hbar\omega_0/3k_BT) - 1]^2}\right] \quad (3)$$

with $\omega_0$ the harmonic wavenumber of the optical model, $\Delta\omega_{d1}(T)$ the decay of the zero-center phonons into two phonons of wavenumber $\omega_1$ and $\omega_2$ (three-phonon process), keeping the sum of $\omega_1 + \omega_2 = \omega_0$ unchanged, $\Delta\omega_{d2}(T)$ the decay into three phonons (four-phonon process), assumed to be of equal wavenumber $\omega_0/3$ for simplicity, and $k_B$ the Boltzmann constant. $A$ and $B$ are anharmonic constants selected as fitting parameters in the calculation and related to the relative probability of the occurrence of each process. The solid curves in Fig. 4 are the calculated phonon

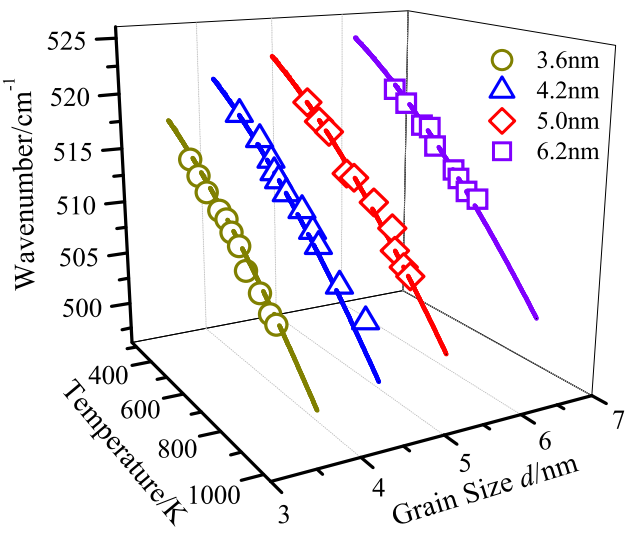


**Figure 4.** Temperature-dependent Raman wavenumber of the $TO_2$ mode in the Si nanocrystals with different grain sizes. The solid curves are the theoretical results with Eqn (3).

wavenumber with temperature using Eqn 3 by varying parameters $\omega_0$, $\omega_1$, $\omega_2$, $A$, and $B$ (listed in Table 1) related to different nanocrystal sizes. The agreement between the theoretical fitting and the experimental data is found to be quite good.

It is well known that the presence of grain boundaries or surfaces leads to a locally lower atomic density and higher structural disorder in comparison to the bulk material. As a result, the quantum confinement effect affects the optical modes at the Brillouin zone center ($q = 0$), because more phonons with $q \neq 0$ (away from Brillouin zone center) contribute to the phonon density of states (DOS) and lead to a red-shift in Raman spectra.[28] The variation of $\omega_0$ with the decrease of grain sizes listed in Table 1, together with the significant harmonic wavenumber shift at smaller sizes shown in Fig. 4, clearly demonstrates the quantum confinement effect where for the particles of larger sizes the wavenumber is not shifted that much. We further present in Fig. 5 an analysis of the Raman spectra using the phonon confinement model[18]

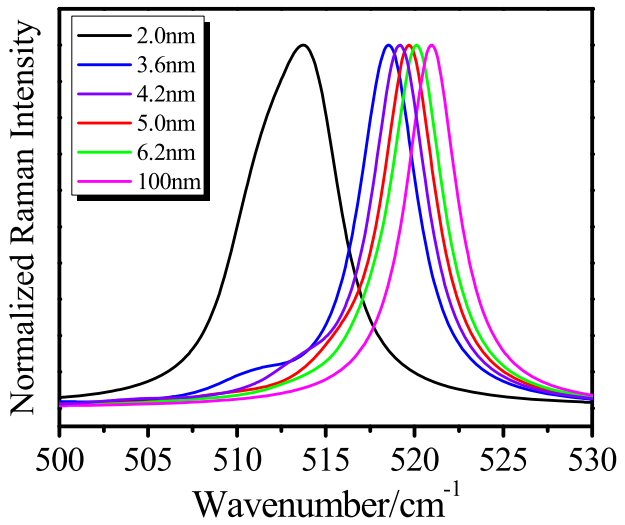


**Figure 5.** Normalized calculated Raman spectra of different grain sizes from the phonon confinement model.

for the different sizes of Si nanocrystals. It is clear that at smaller sizes, there is a significant shift and broadening of the Raman spectra, especially for sizes smaller than 6 nm, while for the particles of larger sizes the peak is not shifted significantly and approaches to the bulk value, which is well consistent with our experimental observation. The asymmetric lineshape in the Raman spectra has also been well reproduced for the Si nanocrystals.

Figure 6(a) shows the variation of linewidths with temperature for the Si nanocrystals of different sizes. The phonon broadening $\Gamma(T)$ mainly comes from the quantum confinement effect and anharmonic decay. Similar to the temperature dependence of Raman peak shift, the phonon broadening can also be described by assuming the decay into two phonons with wavenumber $\omega_1$, $\omega_2$ and the symmetric decay into three phonons[17,29]

$$\begin{aligned}\Gamma(T) &= \Gamma_0 + \Gamma_1 + \Gamma_2 \\ \Gamma_1 &= C\left[1 + \frac{1}{\exp(\hbar\omega_1/k_B T) - 1} + \frac{1}{\exp(\hbar\omega_2/k_B T) - 1}\right] \\ \Gamma_2 &= D\left[1 + \frac{3}{\exp(\hbar\omega_0/3k_B T) - 1} + \frac{3}{[\exp(\hbar\omega_0/3k_B T) - 1]^2}\right]\end{aligned} \quad (4)$$

where $\Gamma_0$ is attributed to the inherent defect or impurity scattering and quantum confinement effect, $\Gamma_1$ is the damping part induced by the asymmetric decay of the three-phonon process, while $\Gamma_2$ represents the four-phonon process, $C$ and $D$ are constants. We have also illustrated in Table 1 the fitting parameters $\Gamma_0$, $C$, and $D$. It is found that $\Gamma_0$ of the $TO_2$ mode in the Si nanocrystals decreases with increasing nanocrystal size, and is close to the corresponding value of 2.8 $cm^{-1}$[30] in the bulk silicon when the Si nanocrystal size is 6.2 nm. This line broadening characteristic agrees well with the peak shift observation in Fig. 4, i.e. demonstrating experimentally that the quantum confinement effect is significant for Si nanocrystals smaller than 6 nm. Furthermore, we notice that the values of $\omega_1 \sim 170\ cm^{-1}$ and $\omega_2 \sim 350\ cm^{-1}$ obtained from Raman peak shift are coincident with those from linewidths, which manifests the asymmetric decay process for the $TO_2$ mode.

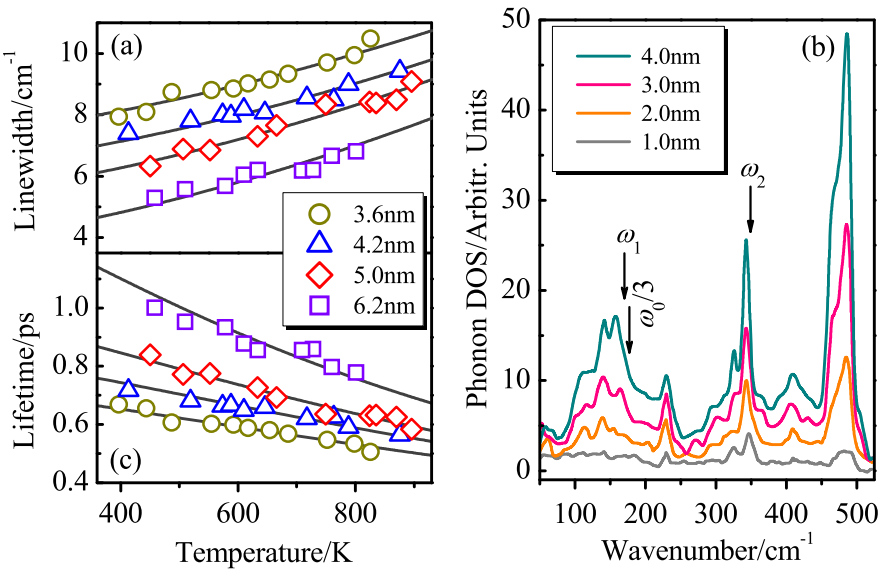


**Figure 6.** (a) Temperature-dependent Raman linewidth $\Gamma(T)$ of the $TO_2$ mode in Si nanocrystals with different grain sizes. The solid curves are the theoretical fitting to Eqn 4. (b) Calculated phonon DOS in Si nanocrystals for different grain sizes reported in [31], with the positions of $\omega_1$, $\omega_2$, and $\omega_0/3$ marked. (c) Temperature-dependent lifetime $\tau(T)$ of the $TO_2$ mode in Si nanocrystals with different grain sizes. The solid curves are the theoretical fitting to Eqn (5).

To exactly understand the decay mechanism, we resort to the calculated (through the generalized Keating model) phonon DOS published in [31] shown in Fig. 6(b) for different Si nanocrystal sizes. We can find a sizable magnitude of the phonon DOS at $\omega_1$ and $\omega_2$ for all these Si nanocrystals, indicating that the asymmetric decay into phonons with wavenumbers near 170 and 350 $cm^{-1}$ is reasonable. The anharmonic constants of *A*, *B*, *C*, and *D* in Table 1 are found to increase with the nanocrystal size. The enhancement of the anharmonic effect can also be observed from the temperature-dependent changes in wavenumbers (Fig. 4) and linewidths [Fig. 6(a)]. In Si nanocrystals, the phonon DOS increases with the nanocrystal size [Fig. 6(b)],[31] resulting in an increase in the probability of inelastic (anharmonic) scattering between phonons. Large numbers of phonons will be produced with increasing temperature, which also leads to the enhanced probability of anharmonic decay of phonons.

From the ratios of *A*/*B* and *C*/*D*, the relative contributions of the three-phonon and four-phonon processes to the total phonon decay can be estimated. From Table 1, it is interesting to note that the ratios of *A*/*B* and *C*/*D* remain almost constant ($7.5 \pm 0.4$) with increasing grain sizes. Although the increasing sizes lead to an enhancement of the phonon DOS, the ratios of magnitude of the phonon DOS of $\omega_1$ ($\omega_2$) to that of $\omega_0/3$ are found to be approximately 1.10 (1.30) for Si nanocrystals (see Fig. 6(b)). As a result, the contribution of the three-phonon and four-phonon processes to the total phonon decay does not change apparently with the increase of the Si nanocrystal sizes. However, the ratios of *A*/*B* and *C*/*D* are much larger than 1.0, indicating that the decay into two phonons is the prevailing process while the four-phonon process makes a minor contribution in the anharmonic coupling of the $TO_2$ mode in Si nanocrystals. This phenomenon is also consistent with the calculated phonon DOS shown in Fig. 6(b), where the weak phonon DOS at $\omega_0/3$ (~174 $cm^{-1}$) shows less probability of the four-phonon process. We can therefore conclude the reliability of our theoretical fitting through the consistency between the variations of *A*/*B* and *C*/*D*.

Finally, it is generally known that the linewidth broadening in Raman scattering is usually related to the lifetime of the decay process of the involved phonons, and we can simply estimate the relaxation time $\tau(T)$ for the decay processes by[32]

$$\Gamma(T) = 1/[2\pi c\tau(T)] = 1/(2\pi c\tau_{\text{elastic}}) + 1/(2\pi c\tau_{\text{inelastic}}) \quad (5)$$

with *c* the velocity of light, $1/(2\pi c\tau_{\text{elastic}})$ ($=\Gamma_0$) from the contribution of elastic scattering, and $1/(2\pi c\tau_{\text{inelastic}})$ ($=\Gamma_1+\Gamma_2$) from the anharmonic scattering. Figure 6(c) displays the lifetimes $\tau(T)$ of the $TO_2$ mode as a function of temperature under different nanocrystal sizes, while the solid curves are the best theoretical fits. We find a significant shortening of $TO_2$ mode lifetime with the increase of the local temperature and decrease of nanocrystal sizes. This is reasonable, because the thermal interaction increases with temperature, which decreases the phonon mean free path at high temperatures, while the decrease of grain size is expected to further enhance the inherent boundary scattering in nanocrystals, which reduces significantly the phonon lifetime.[1]

## Conclusion

The quantum confinement and laser-induced thermal effects have been studied by Raman scattering of nc-Si:H thin films grown by PECVD with different Si nanocrystal sizes (3.6–6.2 nm) in the laser power density range from ~120 to 960 $kW/cm^2$. The observed temperature-dependent wavenumber and linewidth characteristics in Si nanocrystals can be well described by the three-dimensional phonon confinement model, which takes into account both the phonon confinement and the effect of strain, and by the anharmonic effect, which incorporates the three-phonon and four-phonon decay processes. The fitting results exhibit an asymmetrical decay with wavenumbers near 170 and 350 $cm^{-1}$ and the anharmonic effect because of temperature and quantum confinement effect. We have demonstrated experimentally that the quantum confinement effect is dominant for the Raman peak shift and line broadening with Si nanocrystals smaller than 6 nm. Furthermore, it is found that with the increase of the Si nanocrystal sizes the contribution of the three-phonon and four-phonon processes to the total phonon decay does not change apparently, which can be well explained by the phonon DOS in Si nanocrystals.

### Acknowledgements

This work was supported by the National Major Basic Research Project of 2012CB934302, and Natural Science Foundation of China under contracts 10734020, 11074169, and 11174202.

## References

[1] P. Mishra, K. P. Jain, *Phys. Rev. B* **2000**, *62*, 14790.
[2] Y. X. Jie, A. T. S. Wee, C. H. A. Huan, Z. X. Shen, W. K. Choi, *J. Appl. Phys.* **2011**, *109*, 033107.
[3] G. Faraci, S. Gibilisco, A. R. Pennisi, *Phys. Rev. B* **2009**, *80*, 193410.
[4] G. S. Doerk, C. Carraro, R. Maboudian, *Phys. Rev. B* **2009**, *80*, 073306.
[5] A. K. Arora, M. Rajalakshmi, T. R. Ravindran, V. Sivasubramanian, *J. Raman Spectrosc.* **2007**, *38*, 604.
[6] G.Viera, S. Huet, L. Boufendi, *J. Appl. Phys.* **2001**, *90*, 4175.
[7] V. Swamy, *Phys. Rev. B* **2008**, *77*, 195414.
[8] S. Aškrabić, Z. D. Dohčevic-Mitrović, M. Radović, M. Šćepanović, Z. V. Popović, *J. Raman Spectrosc.* **2009**, *40*, 650.
[9] W. Cheng, S. F. Ren, *Phys. Rev. B* **2002**, *65*, 205305.
[10] J. Zi, K. M. Zhang, X. D. Xie, *Phys. Rev. B* **1997**, *55*, 9263.
[11] J. Zi, H. Büscher, C. Falter, W. Ludwig, K. M. Zhang, X. D. Xie, *Appl. Phys. Lett.* **1996**, *69*, 230.
[12] M. Yang, D. M. Huang, P. H. Hao, F. L. Zhang, X. Y. Hou, X. Wang, *J. Appl. Phys.* **1994**, *75*, 651.
[13] M. J. Konstantinović, S. Bersier, X. Wang, M. Hayne, P. Lievens, R. E. Silverans, V. V. Moshchalkov, *Phys. Rev. B* **2002**, *66*, 161311.
[14] A. Torres, A. Martín-Martín, O. Martínez, A. C. Prieto, V. Hortelano, J. Jiménez, A. Rodríguez, J. Sangrador, T. Rodríguez, *Appl. Phys. Lett.* **2010**, *96*, 011904.
[15] R. Tsu and J. G. Hernandez, *Appl. Phys. Lett.* **1982**, *41*, 1016.
[16] T. R. Hart, R. L. Aggarwal, B. Lax, *Phys. Rev. B* **1970**, *1*, 638.
[17] A. Link, K. Bitzer, W. Limmer, R. Sauer, C. Kirchner, V. Schwegler, M. Kamp, D. G. Ebling, K. W. Benz, *J. Appl. Phys.* **1999**, *86*, 6256.
[18] G. Faraci, S. Gibilisco, P. Russo, A. R. Pennisi, S. LaRosa, *Phys. Rev. B* **2006**, *73*, 033307.
[19] B. H. Choi, S. W. Hwang, I. G. Kim, H. C. Shin, Y. Kim, E. K. Kim, *Appl. Phys. Lett.* **1998**, *73*, 3129.
[20] A. Valentin, J. Sée, S. Galdin-Retailleau, P. Dolfus, *J. Phys. Condens. Matter* **2008**, *20*, 145213.
[21] X. Y. Chen, W. Z. Shen, Y. L. He, *J. Appl. Phys.* **2005**, *97*, 024305.
[22] S. Piscanec, M. Cantoro, A. C. Ferrari, J. A. Zapien, Y. Lifshitz, S. T. Lee, S. Hofmann, J. Robertson, *Phys. Rev. B* **2003**, *68*, 241312.
[23] K. H. Li, W. Z. Shen, *J. Appl. Phys.* **2009**, *106*, 063505.
[24] Z. Sui, P. P. Leong, I. P. Herman, G. S. Higashi, H. Temkin, *Appl. Phys. Lett.* **1992**, *60*, 2086.
[25] P. G. Klemens, *Phys. Rev.* **1966**, *148*, 845.
[26] M. Balkanski, R. F. Wallis, E. Haro, *Phys. Rev. B* **1983**, *28*, 1928.
[27] J. F. Kong, W. Z. Shen, Y. W. Zhang, X. M. Li, Q. X. Guo, *Solid State Commun.* **2009**, *149*, 10.
[28] C. C. Yang, S. Li, *J. Phys. Chem. B* **2008**, *112*, 14193.
[29] X. D. Pu, J. Chen, W. Z. Shen, H. Ogawa, Q. X. Guo, *J. Appl. Phys.* **2005**, *98*, 033527.
[30] Z. X. Su, J. Sha, G. W. Pan, J. X. Liu, D. R. Yang, C. Dickinson, W. Z. Zhou, *J. Phys. Chem. B* **2006**, *110*, 1229.
[31] W. X. Zhang, C. Delerue, Y. M. Niquet, G. Allan, E. Wang, *Phys. Rev. B* **2010**, *82*, 115319.
[32] H. F. Liu, N. Xiang, S. Tripathy, S. J. Chua, *J. Appl. Phys.* **2006**, *99*, 103503.